Desalination and Water Treatment
www.deswater.com

doi: 10.5004/dwt.2019.23751

150 (2019) 374–385
May

Adsorptive removal of toxic Methylene Blue and Acid Orange 7 dyes from aqueous medium using cobalt-zinc ferrite nanoadsorbents

Tetiana Tatarchuk[a,b,*], Natalia Paliychuk[b], Rajesh Babu Bitra[c], Alexander Shyichuk[d], Mu. Naushad[e], Ivan Mironyuk[a], Dorota Ziółkowska[d]

[a]*Department of Chemistry, Vasyl Stefanyk Precarpathian National University, Ivano-Frankivsk, 76018, Ukraine, Tel. +38 068 463 24 35, email: tatarchuk.tetyana@gmail.com (T. Tatarchuk)*
[b]*Educational and Scientific Center of Material Science and Nanotechnology, Vasyl Stefanyk Precarpathian National University, Ivano-Frankivsk, 76018, Ukraine, email: nsbu@ukr.net (N. Paliychuk)*
[c]*Department of Physics, G.V.P. College of Engineering for Women, Andhra Pradesh, Visakhapatnam, 530041, India, email: rajeshbabu.bitra@gmail.com*
[d]*Faculty of Chemical Technology and Engineering, UTP University of Science and Technology, Seminaryjna 3, 85–326 Bydgoszcz, Poland, email: szyjczuk@utp.edu.pl (A. Shyichuk)*
[e]*Department of Chemistry, College of Science, Building #5, King Saud University, Riyadh-11451, Saudi Arabia, email: mnaushad@ksu.edu.sa*

Received 19 November 2018; Accepted 6 January 2019

ABSTRACT

Cobalt-zinc ferrite nanoparticles of general formula $Co_{1-x}Zn_xFe_2O_4$ ($0.0 \leqslant x \leqslant 1.0$) were synthesized by means of chemical co-precipitation method. Impedance analysis was used to study the grain and inter-grain conductivities. The changing of complex conductivity with composition confirmed the semiconducting behavior. A significant influence of Zn concentration on dielectric properties was observed. The obtained Co-Zn ferrites were examined as magnetic adsorbents using both cationic and anionic dyes as model pollutants. Substitution of zinc ions with cobalt ones resulted in changes in sorption characteristics. The efficiency of Methylene Blue (MB) dye removal was increased with increasing Co content. On contrary, efficiency of Acid Orange 7 dye removal was increased with increasing Zn content. The adsorption of the both anionic and cationic dyes onto ferrite nanoparticles agreed well with the Langmuir isotherms. The maximum adsorption capacity for the Acid Orange 7 dye was reached up to 31 mg/g using $ZnFe_2O_4$, while the maximum adsorption capacity for the cationic Methylene Blue dye was found to be 3.4 mg/g on $Co_{0.9}Zn_{0.1}Fe_2O_4$. The relation of adsorption efficiency with ionic-covalent and acid-base parameters of the ferrite surface was also discussed.

Keywords: Ferrite nanoparticles; Magnetic sorbents; Dyes; Surface

1. Introduction

Adsorption is well known as affordable and efficient method of water purification. A huge number of sorbents based on diverse materials such as activated carbon, clay minerals, waste biomass, agricultural by-products etc. have been proposed for the removal of various types of pollutants from aqueous medium [1–4]. In the recent decades, literature reports the information about the sorbents with magnetic properties possessing the advantage of after-use separation by means of external magnetic field. Among the magnetic sorbents, the most promising materials are ferrite spinels possessing adjustable crystalline structure [5,6]. Year-to year, spinel ferrite sorbents attract ever increasing attention of

* Corresponding author.

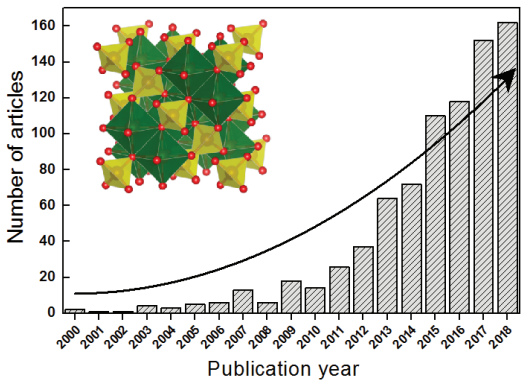

Fig. 1. Number of scientific publications on "ferrites" and "adsorbent" (Source: Scopus®search date: 24–10–2018).

researchers (Fig. 1). Ferrite materials have good chemical and thermal stability. Ferrite sorbents provide fast adsorption kinetics and high adsorption capacity [7]. The raw materials for ferrite synthesis are cheap and readily available [8]. The magnetic spinel materials of micro- and nanometer size have proven to suit well for water decontamination [5,9–14]. The recent examples concern mainly removal of heavy metal ions [15–22] and organic dyes [23–27]. It is important that magnetic properties of the ferrite materials can be finely adjusted via inter-lattice cation substitution [9–13].

Magnetite, Fe_3O_4, is the very popular component of composite magnetic sorbents. As a matter of fact, magnetite is ferrous ferrite, $FeFe_2O_4$, with the spinel crystalline structure. Synthetic magnetite nanoparticles were proved to provide fast and effective removal of Cd(II) ions with adsorption capacity up to 200 mg/g [8]. Inclusion of nanometer-sized magnetite into sorbent matrix provides magnetic properties to the typical sorbents. For example, natural zeolite (clinoptilolite) doped with magnetite particles was proven to be a good sorbent for ^{90}Sr ions [18]. The radionuclide was easily removed using adsorption followed by magnetic separation. Composite sorbent of carbon-magnetite core and zero-valent iron shell was obtained via hydrothermal synthesis and subsequent borohydride reduction [19]. The sorbent consisted of nearly spherical magnetite particles (100–150 nm in size) covered by a carbon layer. Zero-valent iron particles of about 20–25 nm in diameter were aggregated on the carbon surface. The efficient removal of Pb(II) ions (nearly 100%) was achieved due to two subsequent processes: adsorption and reduction by zero-valent iron [19]. Chitosan macromolecules and magnetite nanoparticles were grafted onto graphene oxide surface in order to improve post-sorption separation [20]. The nanometer-sized flakes of the composite sorbent exhibited a good performance in removal of chromate ions from aqueous solutions. The adsorption capacity reached 130 mg/g for 10 h. The weakly bounded Cr ions were removed with alkaline washing. The composite sorbent was retained 80% of its sorption capacity after ten regeneration cycles [20]. Core-shell sorbent of copper and magnetite nanoparticles was obtained using the extract of *Aeglemarmelos* leaves as a reducing and capping agent. The sorbent was used for Pb(II) ions removal [21]. Nanoparticles of carbon sorbent obtained good magnetic properties due to attached nickel ferrite [15]. The adsorption capacity toward mercury ions was registered to be as high as 300 mg/g. Four regeneration cycles result in negligible changes of adsorption and desorption properties [15]. Mixed-phase manganese ferrite and manganese oxide nanoparticles with good magnetic properties were prepared via coprecipitation in alkaline medium [22]. The adsorption capacity toward chromate anions was registered in the range from 30 to 100 mg/g [22]. Magnesium ferrite nanosorbent was obtained using combustion method with glycine-nitrate fuel [16]. The obtained magnetic particles consisted of agglomerates of crystallites approx. 8 nm in size. Good adsorption capacity toward Mn, Co, Ni, and Cu ions was retained after four regeneration cycles [16]. Magnesium ferrite was incorporated into cross-linked alginate beads consisted of agglomerated spherical particles of 10–30 nm in size [17]. The nanosorbent was proved to provide high sorption rate and capacity. Sorption of strontium ions was reached 100 mg/g for approx. 1 h [17].

Much attention is paid by researchers for the adsorption of organic dyes used in textile and printing industries. Typical dye molecules contain toxic aromatic groups and should be removed from the aquatic environment. Magnetic core-shell adsorbent was prepared by grafting chitosan and L-arginine by means of epichlorohydrine on magnetite surface [23]. The carboxyl and amino groups bearing by hair-like chitosan macromolecules grafted with L-arginine provide fast separation of Methyl Orange dye with adsorption capacity as high as 240 mg/g [23]. Three-dimensional flower-like nickel ferrite on the surface of nickel foam was prepared via hydrothermal synthesis [24]. The Congo red dye was adsorbed up to 10 mg/g during 40 min [24]. Magnetic nanometer-sized copper ferrite, $CuFe_2O_4$, was synthesized by the combustion method [25]. Adsorption properties were evaluated using a cationic triarylmethane dye (Malachite Green). The low contact time (~30 min) was sufficient to attain adsorption capacity about 22 mg/g [25]. Phytic acid modified magnetic $CoFe_2O_4$ composites were synthesized by means of one-pot microwave hydrothermal method [26]. The primary nearly spherical (~20 nm) nanoparticles were agglomerated to nanorods and nanoflakes because of magnetic dipolar interactions. As a result, a coral-like nanostructure was formed. Increase of phytic acid amount resulted in decrease of adsorption capacity toward anionic dye and increase of adsorption capacity toward cationic dye. Full magnetic separation of the adsorbent from aqueous solution requires approximately 2 min [26]. A Zn-silica modified $CoFe_2O_4$ nanostructured composite was synthesized using wet chemistry methods [27]. The sorbent comprises clusters of amorphous silica attached to surface of crystalline spinel nanoparticles (approx. 18 nm in size). Using the Methylene Blue dye, the maximum monolayer adsorption was registered to be 25.6 mg/g. Quite effective removal of Cr^{3+}, Cu^{2+} and Pb^{2+} ions was recorded as well. Saturation magnetization of the material (39 emu/g) is sufficient for magnetic removal of the spent sorbent from the decontaminated solution [26].

In the present work, the adsorption properties of cobalt-zinc ferrites were studied thoroughly for the removal of Methylene Blue (MB) and Acid Orange 7 (AO7) dyes. The study is focused on relation of adsorption efficiency with nature of active centers on the surface and inter-grain boundaries and impedance analysis was also used to study grain and inter-grain conductivities.

2. Experimental

2.1. Synthesis and characterization of $Co_{1-x}Zn_xFe_2O_4$ adsorbents

The series of the cobalt-zinc ferrite materials with chemical composition ($Co_{1-x}Zn_xFe_2O_4$, where x ranges from 0.0 to 1.0 with the step of 0.1) were synthesized via co-precipitation method. X-ray diffraction, SEM, EDS, BET, VSM and FTIR spectroscopy were used for characterization of cobalt-zinc ferrite magnetic nanoadsorbents as described in our previous reports [12,13,28]. The room-temperature dielectric studies on the sintered pellets of $Co_{1-x}Zn_xFe_2O_4$ were performed on the Autolab/FRA-2 (Holland) impedance analyzer in the frequency range of 10 Hz to 1 MHz. The dielectric constant can be calculated from the capacitance measured through the two probe method using impedance analyzer. Relation between capacitance and real permittivity is $\varepsilon' = \frac{Cd}{A\varepsilon_0}$, where d is the distance between the two electrodes and A is the area of the sample and ε_0 is the permittivity of the free space. The loss of electromagnetic energy due to absorption and is determined from the expression: $\mathrm{Tan}\delta = \frac{\varepsilon''}{\varepsilon'}$, where ε'' is dielectric loss.

2.2. Determination of point of zero charge

Net surface charge of the sorbent in the aqueous medium was estimated using pH drift method [29]. The initial pH ($pH_{initial}$) of inert electrolyte solution (0.1 M NaCl) was adjusted to a desired value in the range 2.5–11.0 by adding 0.1 M HCl or KOH solutions. Accurately weighted 100 mg of the ferrite powder was added to 15 mL of the solution and the mixture was magnetically stirred for 24 h. The sample was centrifuged and the final pH of the supernatant was measured. The pH meter with combined glass electrode was calibrated immediately before the measurements using standard buffer solutions. The pH difference has positive values at high pH and negative ones at low pH. Values of the final pH were plotted vs. values of the initial pH. The point of zero charge (pH_{PZC}) was determined as intersection of the experimental curve with the straight line $pH_{final} = pH_{initial}$.

2.3. Adsorption measurements

Batch adsorption experiments were carried out in conical flasks with magnetic stirring at ambient temperature (293 K) and neutral pH. Aqueous solutions of MB dye (25 mL) or AO7 dye (50 mL) with pre-set concentration (10; 25; 50; 75; 100 mg/L) were mixed with precisely weighted mass of the sorbent (125 mg or 50 mg, respectively). After stirring overnight, the sorbent was magnetically separated. The equilibrium concentrations of dyes were determined with spectrophotometer (Spectroquant Pharo 300, Merck, Germany) measuring absorbance at 662 nm (MB) or 484 nm (AO7). The optimal wavelengths were determined from the dye spectra (Fig. 2). The adsorption capacity, q_e (mg/g), was calculated as follows [26,30]:

$$q_e = \frac{(C_o - C_e)\cdot V}{m} \quad (1)$$

where q_e is the adsorption capacity (mg/g), C_o and C_e are the initial and the equilibrium dye concentrations (mg/L), m is the adsorbent mass (g) and V is the sample volume (L). The percentage of dye removal was calculated as follows [26]:

$$\text{Removal}\,(\%) = \frac{(C_o - C_f)}{C_o}\times 100 \quad (2)$$

where C_o and C_f are the initial and final dye concentrations, respectively.

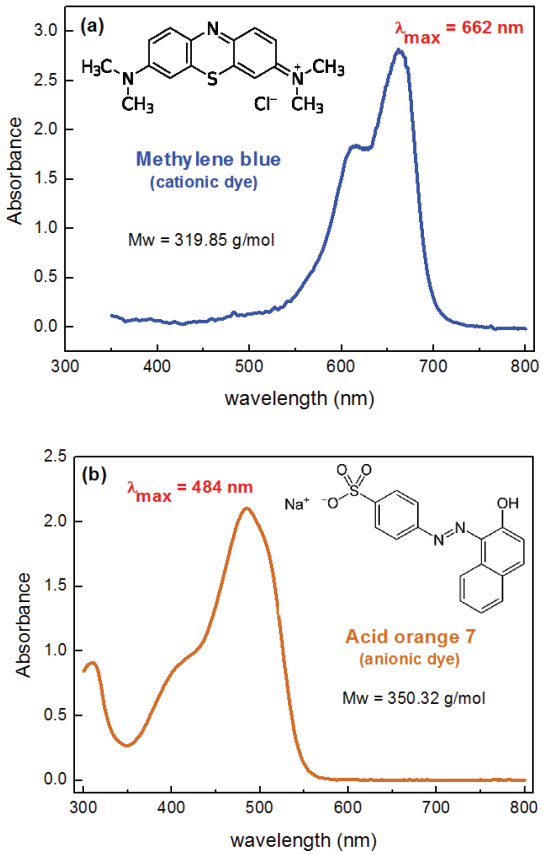

Fig. 2. Molecular structure and absorbance spectra of (a) MB and (b) AO7 dyes.

3. Results and discussion

3.1. Dielectric properties of the $Co_{1-x}Zn_xFe_2O_4$ nanoparticles

3.1.1. Compositional dependence of dielectric constant

The room temperature dielectric constant of Co-Zn nanoferrite with Zn content at frequencies 1 and 10 KHz is shown in Fig. 3. It is observed that substitution of Zn strongly influence the dielectric constant. The dielectric constant rapidly decreases with increasing Zn up to x = 0.6 and thereafter considerable increase is observed beyond x = 0.6.

The variation of dielectric constant with Zn concentration is not a linear function, which suggests that the dielectric constant not only influenced by the substitution of Zn but also on other parameters. In order to facilitate the discussion on variation of dielectric constant; crystallite size, porosity,

inter-ionic bond angles (θ_3, θ_4), and distances between (b, f) ions at octahedral (B) sites are calculated using the relations [9] and listed in Table 1.

It is a well-known fact that, dielectric constant is a direct consequence of electronic exchange between $Fe^{2+} \leftrightarrow Fe^{3+}$ ions and these electrons are transported by means of grains and across the grain boundaries. This results in local displacements of charge carriers which further determine the polarization of the ferrites. The distance between cations present at A-sites (3.6 Å) is greater than that of B-sites (2.9 Å). Therefore, higher the presence of Fe^{2+} and Fe^{3+} concentration at octahedral B sites would enhance the dielectric constant. In mixed spinel ferrite, divalent Zn ions always prefer to occupy the tetrahedral A-sites, Co^{2+} ions to octahedral B-sites, while Fe^{3+} ions occupy both A sites and B-sites but in different proportions to obtain charge neutrality of the system [28]. In the present work, substitution of zinc ions in A-sites will cause migration of some of the Fe^{3+} ions in to B-sites. Thus, one can expect that dielectric constant increases with Zn content due to the availability of Fe^{3+} ions at B sites. In contrast to the above argument, it decreases initially up to x = 0.6 and thereafter, increases with Zn concentration. It can be seen from Table 1 that porosity, inter-ionic distances (b, f) and angles (θ_3, θ_4) increases with Zn content and are responsible to inhibit the exchange between charge carriers between ferrous and ferric ions. However, it is possible for the formation of Fe^{2+} ions to maintain the charge neutrality due to the volatilization Zn. Based on the above discussion, it can be understood that, formation of Fe^{2+} ions takes place in the ferrites when Zn content is above x = 0.6, which further contributes the observed increase in dielectric constant [31,32].

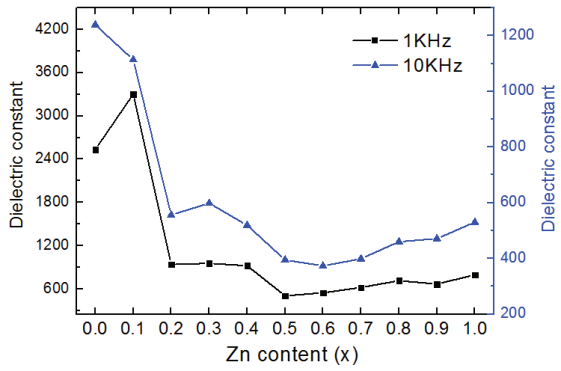

Fig. 3. Compositional dependence of dielectric constant at different frequencies.

3.1.2. Frequency dependence of dielectric constant and loss tangent

Frequency response of the ε′ and loss tangent (Tan δ) for all Zn substituted *Co* ferrite samples at room temperature are shown in Fig. 4.

It can be seen (Fig. 4) that both ε′ and Tan δ shows similar response to the applied frequency i.e., decreases with increasing frequency, which is a normal dielectric behavior of spinel ferrites. The dispersion is rapid at lower frequencies and independent at high-frequencies. The present variation can be understood from Koop's phenomenological theory [33], the ferrite ceramic assumed to be composed of well conducting grains separated by highly resistive layers or grain boundaries. Therefore, electrons are pile up at the grain boundaries which enhance the dielectric constant. In the same line, the observed high loss at lower frequencies is due to requirement of greater energy for the exchange of electron between the Fe^{2+} and Fe^{3+} ions. However, in the high-frequency region, grain boundaries are less effective and therefore smaller energy is required for electron transfer between Fe^{2+} and Fe^{3+} ions, which is responsible for lower loss. Further, exchange of charge carriers reduced at higher applied frequencies, which is responsible for the observed decrease in dielectric constant.

Table 1
Dielectric constant (ε′), crystallite size (*D*), specific surface area (*S*), porosity, inter-ionic bond angles (θ_3, θ_4) and distances (b,f) between ions at octahedral (*B*) sites (data taken from reference [28])

Zn (*x*)	Dielectric constant (ε′) at 300 K				S_{BET}	Porosity (%)	*D* (nm)	θ_3	θ_4	b	f
	1 KHz	10 KHz	100 KHz	1,000 KHz							
0	2534.9	1238.9	672.5	366.3	9.7	2.9	28	90.26	125.32	2.9535	5.1155
0.1	3301.4	1113.3	638.4	305.3	11	3.6	36	91.61	125.6	2.9626	5.1313
0.2	940.6	556.4	446.2	325.8	9.8	6.1	47	91.7	125.66	2.9662	5.1376
0.3	953.9	598.3	384.8	257.1	10.2	5.3	50	91.5	125.61	2.9692	5.1428
0.4	922.9	519.2	434.9	325.1	10.1	9.7	54	91.54	125.62	2.9704	5.1449
0.5	503.9	394.9	376.1	306.3	8.2	12.9	51	91.8	125.68	2.9723	5.1481
0.6	546.8	373.3	337.9	251.8	8.2	15.1	45	91.78	125.68	2.9741	5.1513
0.7	619.5	398.8	360.1	278.1	9.8	19.1	44	92.04	125.73	2.9785	5.1589
0.8	714.8	460.2	415.6	320.9	9	22	40	92.97	125.94	2.9774	5.157
0.9	666.8	471.1	423.1	339.5	8.6	26.7	38	93.92	126.15	2.9813	5.1638
1	797.1	530.3	429.9	326.6	7	28.7	37	94.33	126.24	2.9837	5.168

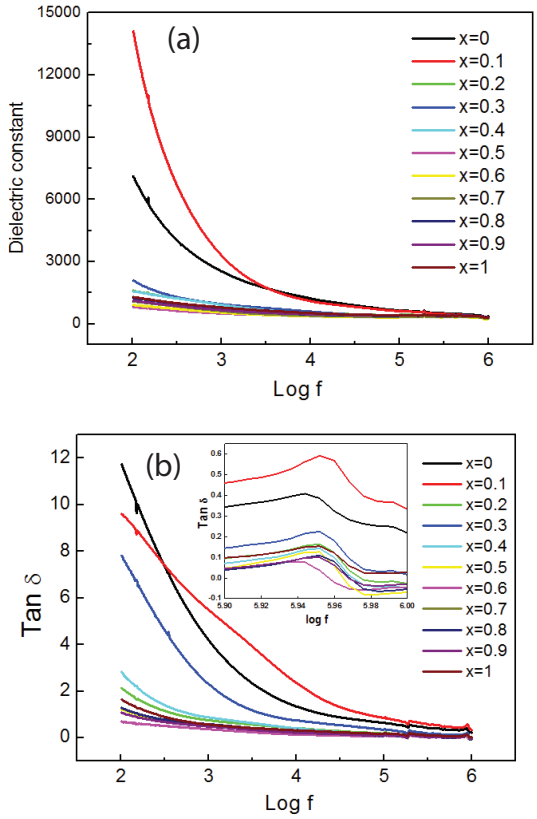

Fig. 4. Frequency dependence of (a) dielectric constant and (b) loss tangent.

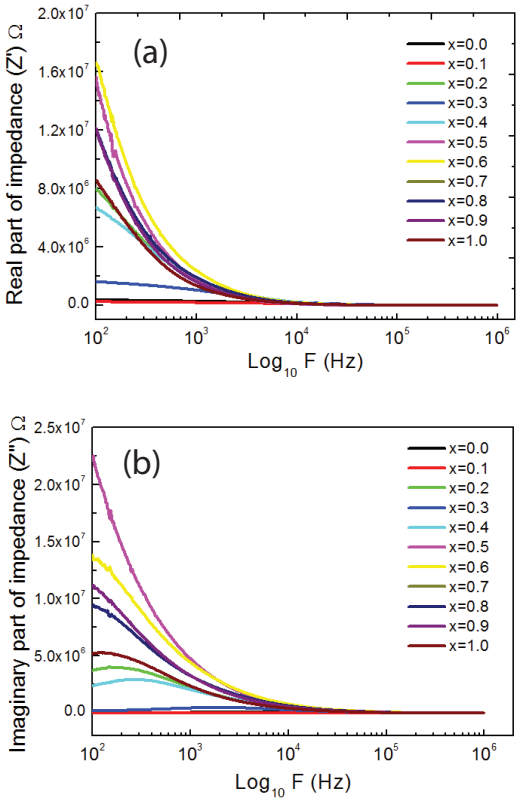

Fig. 5. Room temperature (a) real and (b) imaginary complex impedance as a function of frequency.

3.1.3. Impedance spectroscopy analysis

Electrical conductivity of ferrites is influenced by the type and amount of cations present in the material, porosity, and grain size. However, grain size/grain boundary plays a major role in conductivity mechanism. Impedance spectroscopy is a very simple tool to understand and separate the contribution from grain and grain boundaries to the conduction mechanism [34]. The classical model to describe the impedance behavior is that of Debye and it is written in the form [34]:

$$Z^{*} = Z' + iZ'' = \frac{R}{(1 + i\omega\tau)} \tag{3}$$

where $Z' = R/[1 + (\omega RC)^2]$ is the real part of complex impedance, $Z'' = \omega R^2 C/[1 + (\omega RC)^2]$ is the imaginary part of complex impedance, ω is the angular frequency and $\tau = RC$ is the relaxation time. Figs. 5(a) and (b) show the frequency dependent Z' and Z'' at room temperature for different Zn concentrations respectively. It is evident from the plot (5(a)) that the values of Z' decreases with increasing applied frequency, suggest the enhancement in AC conductivity at higher frequency. It can also be seen that for the Zn concentration x = 0.6 maximum Z' is obtained and decreases again thereafter, which is consistent with dielectric data (Fig. 3).

The Nyquist plots from complex impedance data of Co-Zn ferrite has been shown in Fig. 6. In general, Nyquist plot typically shows two semicircles; the first semicircle at low frequency side is due to the contribution of the grain boundary and second semicircle at high frequency is due to the grain or bulk properties of the materials. It is clear from Fig. 6 that no complete semicircle is found for all the samples. Moreover, for the composition x = 0.5 (Zn) onwards, only one quarter circle/arc is observed. It is because of the predominance of grain boundary resistance and grain resistance is not possible to resolve within the applied filed range. Similar behavior is reported in the literature in different ferrites [35]. The diameter of the semicircles is a measure of the resistance of the grain and grain boundaries. The diameters of the semicircle (Fig. 6) suggest the resistance contribution is purely from the grain interior and grain boundary. It can also be seen from complex plane plot that grain boundary resistance increases with increase in Zn concentration.

3.2. Adsorption mechanism

Surface charge of the samples has a marked effect on the adsorption ability and adsorption mechanism. Ferrite materials were known to adsorb both cationic and anionic species from aqueous solutions. Net surface charge is a useful parameter to estimate nature of active centers on the adsorbent surface. The surface charge of the ferrite sorbents was changed at different pH. The surface was positively charged in acid medium or negatively charged in alkaline medium. The pH at which the surface has zero net charge, known as pH_{pzc} which is characteristic of amphoteric surface.

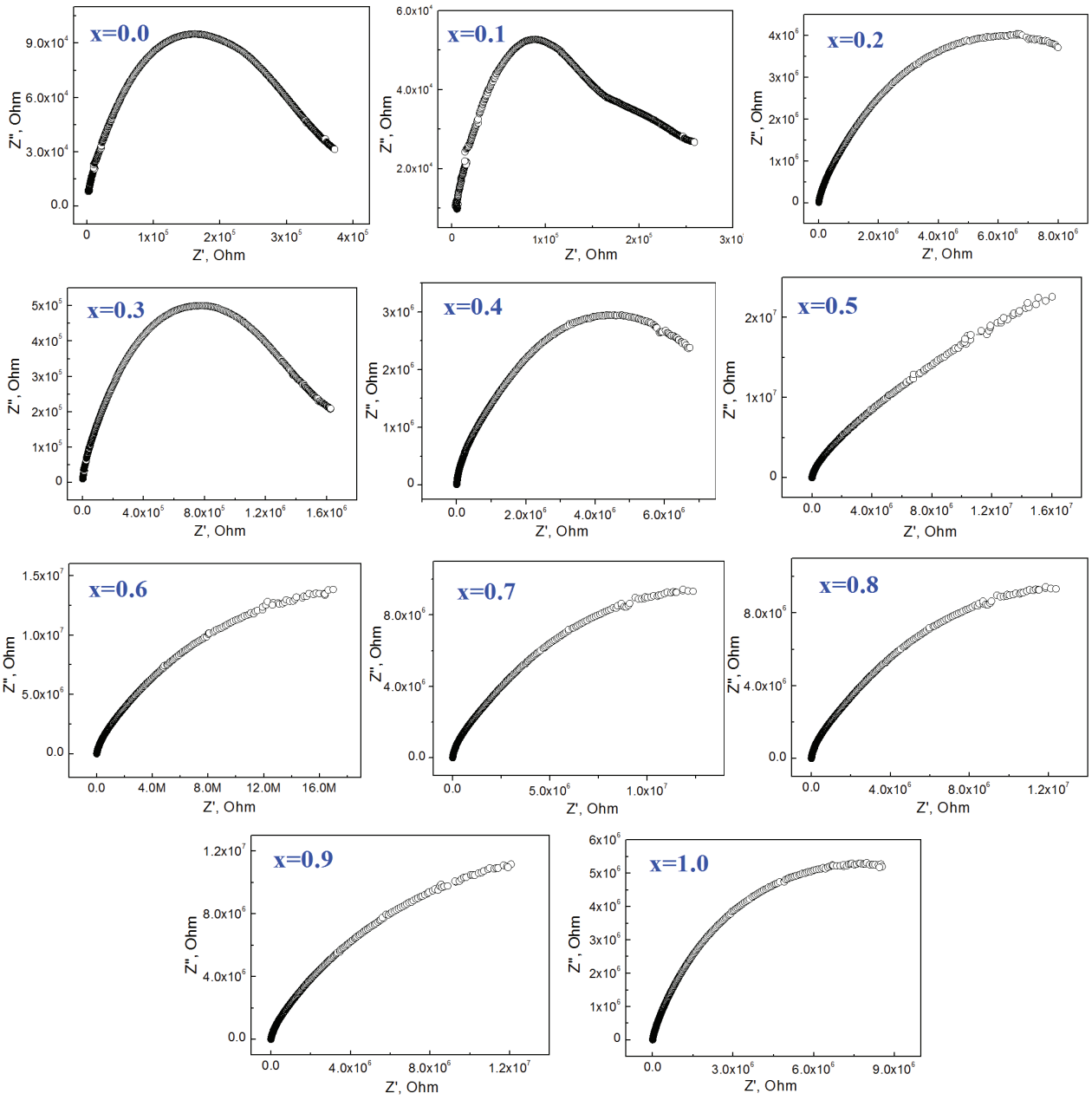

Fig. 6. Impedance spectra of cobalt-zinc ferrites at room temperature.

The value of pH_{pzc} is determined by the type and concentration of surface sites. The illustrative data is presented in Fig. 7 using the samples with x = 0.0, 0.1, and 0.5. When the pH is higher than the PZC of the samples, their surface becomes negatively charged. In this case, electrostatic interaction with cationic species (for example, MB) was favorable. On contrary, the surface charge became positive in a solution with pH value lower than the PZC. In that case, electrostatic attraction of anionic species (for example, AO7) prevails. The reaction of protonation and deprotonation could be described by the following equations [36]:

$$=M-OH+H^{+}\xrightarrow{\text{protonation}}=M-OH_2^{+}\left(pH<pH_{PZC}\right) \quad (4)$$

$$=M-OH+OH^{-}\xrightarrow{\text{deprotonation}}=M-O^{-}+H_2O\left(pH>pH_{PZC}\right) \quad (5)$$

The measured values of the pH_{PZC} were in the range from 6.98 to 7.61 (Table 2). The zinc content had negligible effects on pH_{PZC} of the studied samples. Moreover, the plots of final pH vs. initial pH of all the samples had plateau (Fig. 7). In other words, the value of pH_{final} was almost unchanged at any value of $pH_{initial}$ in this range. In the range pH = 6.98–7.61, the ferrite surface has buffering properties. The amphotheric nature of the ferrite surface is illustrated in Fig. 8 [36]. Hence, at natural pH the surface was able to adsorb both anionic and cationic species via electrostatic interaction. In the present

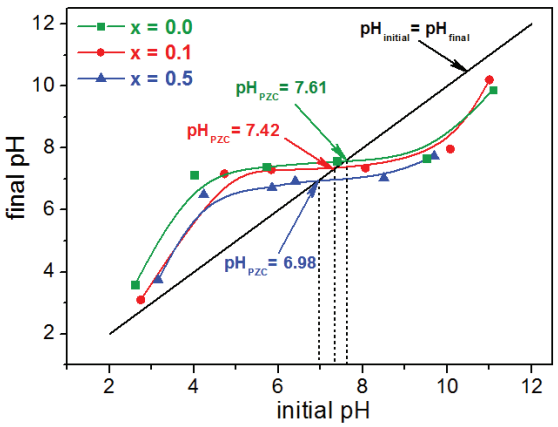

Fig. 7. Determination of zero point charge (pH_{ZPC}) of ferrites $Co_{1-x}Zn_xFe_2O_4$. The values of final pH were plotted vs. initial pH (three most representative samples with x = 0.0, 0.1, 0.5 are shown) (conditions: NaCl concentration 0.1 mol/L, adsorbent mass 100 mg, V = 15 mL).

Table 2
Point of zero charge (PZC) of the $Co_{1-x}Zn_xFe_2O_4$ ferrites (conditions: NaCl concentration 0.1 mol/L, adsorbent mass 100 mg, V = 15 mL)

X	pH_{PZC}
0.0	7.61
0.1	7.42
0.2	7.43
0.3	7.59
0.4	7.38
0.5	6.98
0.6	7.28
0.7	7.45
0.8	7.50
0.9	7.41
1.0	7.42

study, both anionic and cationic dyes were used to estimate adsorption activity of the zinc-cobalt ferrites. The obtained experimental data (Figs. 9 and 10) revealed that adsorption of MB dye on the zinc-cobalt ferrites was significantly lower than adsorption of AO7 dye. Thus, the adsorption was higher for the anionic species than for cationic one.

The equilibrium isotherms give important information about the sorption mechanism and the features of interaction on the surface. Taking in mind the amphoteric character of cobalt-zinc ferrites surface, the adsorption isotherms were determined at nearly neutral pH. The data in Figs. 9 and 10 indicate relationships between adsorption capacity (mg/g) and the equilibrium dye concentration (mg/L). The samples with x = 0.7….1.0 revealed low adsorption capacity for MB and for that reason they were not used in the equilibrium adsorption studies with high concentration of MB solutions. The Langmuir, Freundlich, and Dubinin-Radushkevich theoretical models were used to analyze the obtained isotherms (Fig. 11 and Table 3).

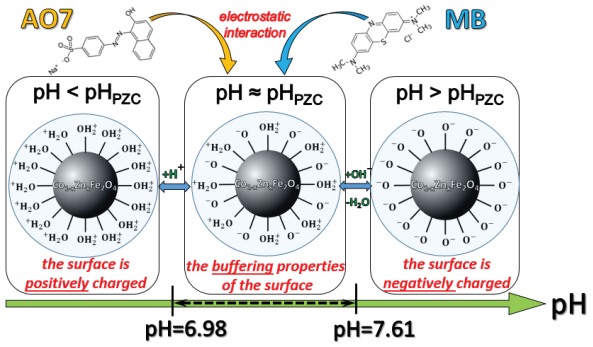

Fig. 8. Schematic illustration of buffering properties of the cobalt-zinc ferrites surface.

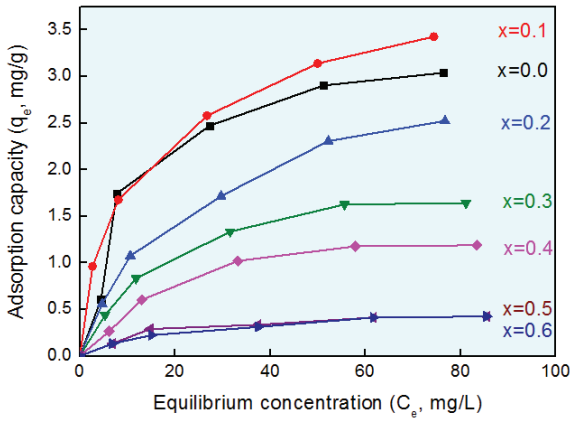

Fig. 9. Equilibrium isotherms of Methylene Blue dye adsorption on the cobalt-zinc ferrite samples with different substitution degree (conditions: volume of dye solution 25 mL, adsorbent dosage 125 mg, natural pH, temperature 20°C).

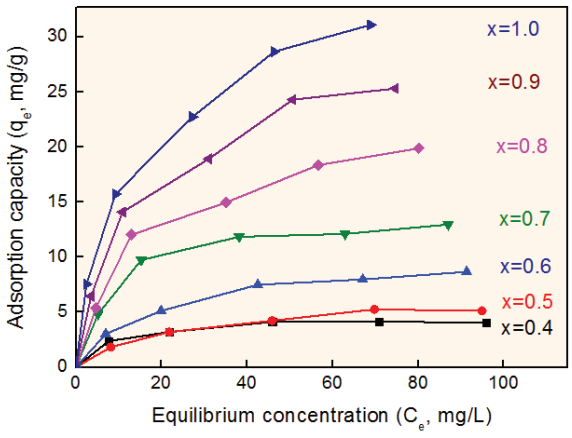

Fig. 10. Equilibrium isotherms of Acid Orange 7 dye adsorption on the cobalt-zinc ferrite samples with different substitution degree (conditions: volume of dye solution 50 mL, adsorbent dosage 50 mg, natural pH, temperature 20°C).

The Langmuir model assumes that (i) monolayer adsorption takes place, (ii) the adsorbent's active sites are identical and (iii) no interaction between the adsorbed

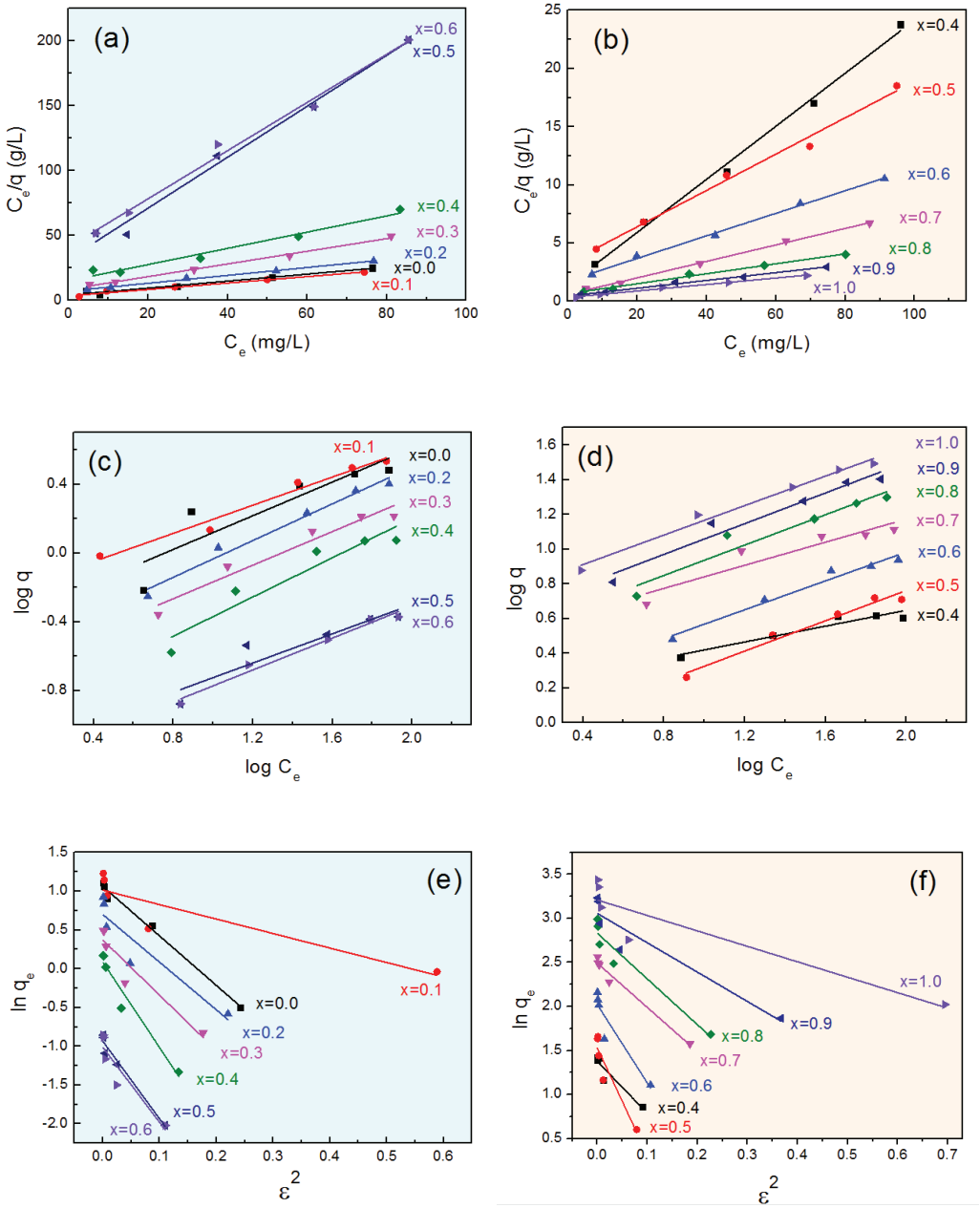

Fig. 11. (a,b) Langmuir's plot of the *Ce*/*q* vs. *Ce*, (c,d) Freundlich's plot of the log *q* vs. log *Ce* and (e,f) Dubinin-Radushkevich's plot of the ln q_e vs. ε² of the cobalt-zinc ferrites for Methylene blue solution (a,c,e) and for Acid orange 7 solution (b,d,f).

molecules occurs [37]. Two forms of the Langmuir equation are the following [38]:

$$q_e = \frac{q_{\max} K_L C_e}{1 + K_L C_e} \left(\text{non-linear form}\right) \tag{6}$$

$$\frac{C_e}{q_e} = \frac{C_e}{q_{\max}} + \frac{1}{K_L q_{\max}} \left(\text{linear form}\right) \tag{7}$$

where q_e (mg/g) refers the equilibrium mass of dye adsorbed per unit adsorbent mass, C_e (mg/L) is the equilibrium dye concentration, K_L (L/g) and q_m (mg/g) are the isotherm constants. Linear dependences of C_e/q_e vs. C_e were plotted for each sample (Figs. 11(a) and (b)). Figs. 11(a) and (b) show clearly that the adsorption of MB and AO7 dyes onto ferrite samples was well described with the Langmuir model. The values of the Langmuir constants q_m and K_L are presented in Table 3 together with the correlation coefficients (R^2). The maximum adsorption capacity for MB was decreased from 3.04 to 0.43 mg/g with the increase in Zn content from $CoFe_2O_4$ to $Co_{0.4}Zn_{0.6}Fe_2O_4$. At the same time, the maximum adsorption capacity for AO7 was increased with increase of Zn content from 1.07 (for $CoFe_2O_4$) to 31.12 mg/g (for $ZnFe_2O_4$). A dimensionless constant, commonly known as separation factor (R_L), can be represented as follow [39]:

Table 3
Adsorption model parameters

Sample	$q_{max,exp}$ (mg/g)	Langmuir model				Freundlich model			Dubinin-Radushkevich model			
		$q_{max,calc}$ (mg/g)	b	R_L (L/mg)	R^2	K_F (mg/g(mg/L)$^{1/n}$)	$1/n$	R^2	$q_{max,calc}$ (mg/g)	β (mol^{2}Kj^{-2})	E (kJ mol^{-1})	R^2
Methylene blue												
X = 0.0	3.04	3.70	4.09	0.142	0.973	0.43	0.49	0.802	2.89	6.38	0.28	0.990
X = 0.1	3.43	4.02	3.44	0.131	0.996	0.61	0.41	0.986	2.76	1.87	0.52	0.826
X = 0.2	2.52	3.28	7.14	0.208	0.995	0.27	0.53	0.978	2.02	6.15	0.29	0.867
X = 0.3	1.64	2.05	8.60	0.165	0.995	0.22	0.49	0.948	1.45	7.12	0.27	0.910
X = 0.4	1.19	1.59	15.09	0.212	0.972	0.12	0.57	0.909	1.09	11.03	0.21	0.953
X = 0.5	0.43	0.51	31.84	0.156	0.989	0.10	0.59	0.924	0.39	10.02	0.22	0.970
X = 0.6	0.43	0.54	41.20	0.202	0.991	0.06	0.46	0.979	0.36	9.69	0.23	0.867
Acid orange 7												
X = 0.0	1.70	2.04	9.43	0.161	0.986	0.26	0.43	0.940	1.56	15.53	0.18	0.911
X = 0.1	1.96	2.72	13.87	0.274	0.994	0.16	0.57	0.964	1.70	20.56	0.16	0.923
X = 0.2	2.13	3.11	14.94	0.318	0.998	0.15	0.60	0.980	1.77	21.32	0.15	0.901
X = 0.3	2.96	3.99	7.63	0.233	0.990	0.30	0.52	0.969	2.64	17.36	0.17	0.893
X = 0.4	4.16	4.39	1.36	0.056	0.996	1.55	0.23	0.915	3.97	5.90	0.29	0.885
X = 0.5	5.25	6.41	3.28	0.173	0.991	0.77	0.44	0.970	4.63	12.19	0.20	0.888
X = 0.6	8.67	10.32	1.75	0.153	0.997	1.42	0.42	0.974	7.55	8.90	0.24	0.874
X = 0.7	12.97	14.12	0.60	0.078	0.998	3.22	0.33	0.879	12.09	5.03	0.32	0.978
X = 0.8	19.89	23.36	0.66	0.133	0.992	3.15	0.44	0.935	16.98	5.20	0.31	0.931
X = 0.9	25.34	29.85	0.45	0.120	0.993	4.13	0.44	0.959	21.26	3.33	0.39	0.897
X = 1.0	31.12	35.84	0.33	0.105	0.992	5.52	0.42	0.985	24.75	1.76	0.53	0.850

$$R_L = \frac{1}{1 + K_L C_o} \tag{8}$$

with K_L (L/mg) is the Langmuir constant and C_o is the initial concentration of adsorbate (mg/L). The adsorption nature may be estimated as unfavorable, linear, favorable or irreversible in the case the R_L values are $R_L > 1$; $R_L = 1$; $0 < R_L < 1$ or $R_L = 0$, respectively. In the present study, all the calculated R_L values were in the range $0 < R_L < 1$ (Table 2) indicated the adsorption nature was favorable for both MB and AO7 dyes.

The Freundlich model [40] describes multilayer sorption and sorption on heterogeneous surfaces with no a finite adsorption value. The Freundlich equations may be presented as follow [40]:

$$q_e = K_F C_e^{1/n} \left(\text{non-linear form}\right) \tag{9}$$

$$\ln q_e = \ln K_F + \frac{1}{n} \ln C_e \left(\text{linear form}\right) \tag{10}$$

where q_e is the adsorption value (mg/g), C_e is the equilibrium dye concentration (mg/L), K_F and $1/n$ are model parameters. The parameter K_F (mg/g) is the characteristic of adsorption capacity and $1/n$ represents adsorption strength. The Freundlich constants K_F and $1/n$ are calculated from the intercept and slope of a linear plot of ln q_e vs. ln C_e. The value of $1/n$ below 1 implies chemisorption process and indicate heterogeneity of active centers. The adsorption nature is more heterogeneous in the case $1/n$ is close to zero. The value of $1/n < 1$ indicates favorable adsorption [37,41]. The obtained values of the Freundlich constants are presented in Table 3. The $1/n$ values were between 0 and 1 indicated favorable adsorption of both dyes onto ferrite surface. Larger values of the K_F constant indicated increased affinity of the Co-Zn ferrite nanoparticles toward the AO7 dye (Table 3).

The Dubinin–Radushkevich (D-R) empirical model [37] is usually used to distinguish between physical and chemical nature of the adsorption process. The linear form of Dubinin–Radushkevich isotherm may be presented as follows [37]:

$$\ln q_e = \ln q_{max} - \beta\varepsilon^2 \tag{11}$$

where q_{max} (mg/g) is the D-R monolayer capacity, β (mol^2/kJ^2) is the activity coefficient and ε is the Polyani potential. Values of ε can be calculated from the following equation [37]:

$$\varepsilon = RT \ln\left[1 + \left(\frac{1}{C_e}\right)\right] \tag{12}$$

where the gas constant R = 8.314 J/(mol K) and temperature T (in K).

The coefficient β is used to calculate mean sorption energy, E (kJ/mol) [37]:

$$E = \frac{1}{\sqrt{2\beta}} \quad (13)$$

The E value indicates mean free energy needed to transfer one mole of sorbate from infinity to the adsorbent surface. It gives information about the adsorption mechanism. The physical adsorption takes place in the case E value is less than 8 kJ/mol. The adsorption has rather chemical nature in the case E value is in the range of 8–16 kJ/mol. The experimental plots of ln q_e vs. ε^2 proved to be quite straight lines (Figs. 11(e) and (f)). Correspondingly, the values of D-R parameters were calculated (Table 3). The obtained values of adsorption energy were below 8 kJ/mol indicated physical (electrostatic) sorption mechanism for all the ferrite sorbents studied. In the case of MB adsorption, the highest value of E (0.52 kJ/mol) was observed for the sample with x = 0.1. In the case of AO7 adsorption, the maximum energy of interaction between the dye molecules and adsorbent surfaces (0.53 kJ/mol) was observed for the sample with x = 1.0.

The data of Table 3 show that the adsorption of the dyes onto cobalt-zinc ferrites was better fitted to the Langmuir model (R^2 = 0.972 ÷ 0.996 for MB and R^2 = 0.986 ÷ 0.998 for AO7) than the Freundlich and Dubinin-Radushkevich models. The results indicated rather homogenous nature of the adsorbent surface. The results Dubinin-Radushkevich model confirmed that dominating adsorption mechanism was electrostatic interaction between the surface of the adsorbent and charged part of the dye molecules (Figs. 9 and 10).

All the zinc-cobalt ferrites revealed larger adsorption affinity for the AO7 dye as compared with pure cobalt ferrite (Fig. 12). In other words, the adsorption activity of ferrites regarding anionic dye was enhanced with the increase of the degree of zinc substitution. This fact may be explained as a result of increase of concentration of Fe^{3+} ions in the B-sites and/or increase of concentration of Zn^{2+} ions in the tetrahedral sites of the ferrite lattice.

At first time, we used ionic-covalent parameter (ICP) proposed by Portier [42] for evaluation of acidic properties of cobalt-zinc ferrites. The ionic-covalent balance of chemical bonds in the mixed oxide affects both physical and chemical properties [43], and adsorptive properties as well. Our previous published data showed that the Zn ions occupied tetrahedral sites of the ferrite sub-lattice, while Co and Fe ions occupied both octahedral and tetrahedral sites [28]. Thus, the summary ICP of ferrites $Co_{1-x}Zn_xFe_2O_4$ was calculated by the following equation [42]:

$$\begin{aligned}\Sigma ICP = {} & c\left(Zn_A^{2+}\right)\cdot ICP\left(Zn_A^{2+}\right) + c\left(Co_A^{2+}\right)\cdot ICP\left(Co_A^{2+}\right) \\ & + c\left(Fe_A^{3+}\right)\cdot ICP\left(Fe_A^{3+}\right) + c\left(Co_B^{2+}\right)\cdot ICP\left(Co_B^{2+}\right) \\ & + c\left(Fe_B^{3+}\right)\cdot ICP\left(Fe_B^{3+}\right)\end{aligned} \quad (14)$$

where c is the concentration of cations and ICP is the partial ionic-covalent parameter of each cation in A- or B-sites of the spinel lattice. The ICP values were calculated from the following equation [42]:

$$ICP = \log P - 1.38\chi + 2.07 \quad (15)$$

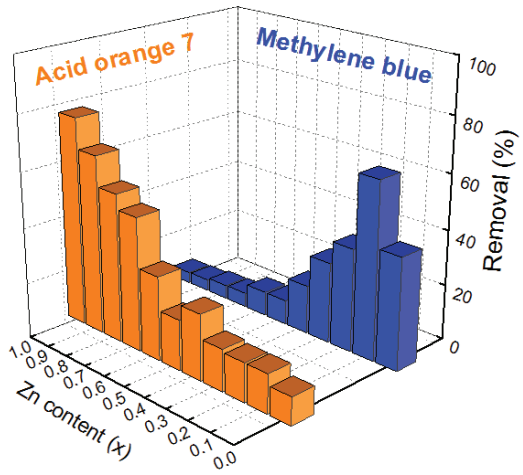

Fig. 12. Removal efficiencies of MB and AO7 from 10 mg/L solution of dye onto cobalt-zinc ferrites.

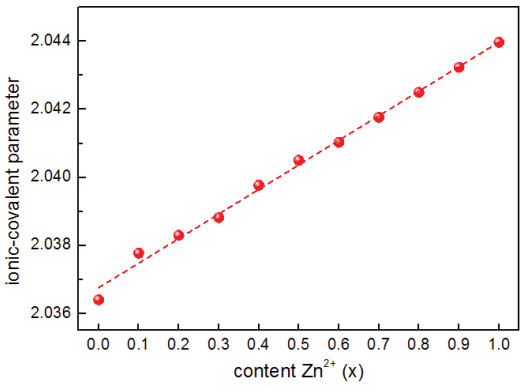

Fig. 13. Ionic-covalent parameter vs. Zn content.

Polarizing power of the cation, P, is calculated as $P = Z/r^2$ using Z (formal cation charge) and r (the Shannon ionic radius taking into account the coordination of the cation [44]). The value of χ is electronegativity depending from cation oxidation state [45]. The increase in zinc content led to increase of Σ ICP and indicated the increase of acidic character of the cobalt-zinc ferrite surface (Fig. 13).

4. Conclusions

Sorption properties of cobalt-zinc ferrites $Co_{1-x}Zn_xFe_2O_4$ ($0.0 \leqslant x \leqslant 1.0$) were investigated in regard to ionic-covalent parameter and dielectric characteristic. The adsorption of AO7 dye on the cobalt-zinc ferrite surface was increased with increasing zinc content. The adsorption mechanism of both MB and AO7 dyes was electrostatic interactions between the adsorbate and adsorbent surface. The surface of cobalt-zinc ferrite becomes more acidic with increase of zinc content. Adsorption efficiency of the mixed ferrites for AO7 dye was increased with increase in zinc content and this was attributed to the increase of ionic-covalent parameters of ferrites and acidity of the surface. The $ZnFe_2O_4$ ferrite showed the largest adsorption capacity to AO7 (31.12 mg/g) and could be used as efficient adsorbent for the removal of

anionic dyes from wastewaters. The obtained results are important for the practical application of transition metal substituted magnetic ferrites in the water treatment. All the mixed ferrites have dielectric constant lower than the pure cobalt ferrite. The overall decreasing trend in dielectric constant suggested that zinc ions obstructed hopping of charge carriers by ferrous and ferric ions. Complex impedance data confirmed that grain boundary resistance was increased with increasing the zinc ion content.

Acknowledgements

This work was supported by the Ukrainian Ministry of Education and Science (Project MESU 0118U000254 and 0117U002408).

References

[1] Z.A. ALOthman, R. Ali, M. Naushad, Hexavalent chromium removal from aqueous medium by activated carbon prepared from peanut shell: adsorption kinetics, equilibrium and thermodynamic studies, Chem. Eng. J., 184 (2012) 238–247.
[2] M. Naushad, T. Ahamad, G. Sharma, M.M. Alam, Z.A. ALOthman, S.M. Alshehri, A.A. Ghfar, Synthesis and characterization of a new starch/SnO_2 nanocomposite for efficient adsorption of toxic Hg^{2+} metal ion, Chem. Eng. J., 300 (2016) 306–316.
[3] A.B. Albadarin, Maurice N. Collins, M. Naushad, Saeed Shirazian, Activated lignin–chitosan extruded blends for efficient adsorption of methylene blue, Chem. Eng. J., 307 (2017) 264–272.
[4] I.F. Mironyuk, V.M. Gun'ko, H.V. Vasylyeva, O.V. Goncharuk, T.R. Tatarchuk, V.I. Mandzyuk, N.A. Bezruka, T.V. Dmytrotsa, Effects of enhanced clusterization of water at a surface of partially silylated nanosilica on adsorption of cations and anions from aqueous media, Microporous. Mesoporous. Mater., 277 (2019) 95–104.
[5] D. Harikishore Kumar Reddy, Yeoung-Sang Yun, Spinel ferrite magnetic adsorbents: alternative future materials for water purification?, Coord. Chem. Rev., 315 (2016) 90–111.
[6] T. Tatarchuk, M. Bououdina, B. Al-Najar, R.B. Bitra, Green and Ecofriendly Materials for the Remediation of Inorganic and Organic Pollutants in Water. In: Naushad M. (eds) A New Generation Material Graphene: Applications in Water Technology., Springer, Cham, 2019, pp. 69–110.
[7] A.A. Alqadami, M. Naushad, Z.A. ALOthman, A.A. Ghfar, Novel metal–organic framework (MOF) based composite material for the sequestration of U (VI) and Th (IV) metal ions from aqueous environment, ACS. Appl. Mat. Interf. 9 (2017) 36026–36037.
[8] F. Liu, K. Zhou, Q. Chen, A. Wang, W. Chen, Preparation of magnetic ferrite by optimizing the synthetic pH and its application for the removal of Cd(II) from Cd-NH_3-H_2O system, J. Mol. Liq., 264 (2018) 215–222.
[9] T. Tatarchuk, M. Bououdina, J.J. Vijaya, J.L. Kennedy, Spinel Ferrite Nanoparticles: Synthesis, Crystal Structure, Properties, and Perspective Applications. In: Fesenko O., Yatsenko L. (eds) Nanophysics, Nanomaterials, Interface Studies, and Applications. NANO 2016. Springer Proceedings in Physics, Springer, Cham, 195 (2017) 305–325.
[10] A. Abu El-Fadl, A.M. Hassan, M.H. Mahmoud, Tetiana Tatarchuk, I.P. Yaremiy, A.M. Gismelssed, M.A. Ahmed, Synthesis and magnetic properties of spinel $Zn_{1-x}Ni_xFe_2O_4$ ($0.0 \le x \le 1.0$) nanoparticles synthesized by microwave combustion method, J Magn. Magn. Mater., 471 (2019) 192–199.
[11] S. Raghuvanshi, S.N. Kane, T.R. Tatarchuk, F. Mazaleyrat, Effect of Zn addition on structural, magnetic properties, antistructural modeling of $Co_{1-x}Zn_xFe_2O_4$ nano ferrite, AIP Conf. Proc., 1953 (2018) 030055.
[12] T.R. Tatarchuk, N.D. Paliychuk, M. Bououdina, B. Al-Najar, M. Pacia, W. Macyk, A. Shyichuk, Effect of cobalt substitution on structural, elastic, magnetic and optical properties of zinc ferrite nanoparticles, J. Alloys. Compd., 731 (2018) 1256–1266.
[13] T. Tatarchuk, M. Bououdina, W. Macyk, O. Shyichuk, N. Paliychuk, I. Yaremiy, B. Al-Najar, M. Pacia, Structural, optical, and magnetic properties of Zn-doped $CoFe_2O_4$ nanoparticles, Nanoscale. Res. Lett., 12 (2017) 141–151.
[14] M. Naushad, M.A. Abdalla, T. Ahmad, Z.A. ALOthman, S.M. ALShehri, A.A. Ghfar, Efficient removal of toxic metal ions from wastewater using a recyclable nanocomposite: a study of adsorption parameters and interaction mechanism, J. Cleaner. Prod., 156 (2017) 426–436.
[15] M. Naushad, T. Ahamad, B.M. Al-Maswari, A.A. Alqadami, SM. Alshehri, Nickel ferrite bearing nitrogen-doped mesoporous carbon as efficient adsorbent for the removal of highly toxic metal ion from aqueous medium, Chem. Eng. J, 330 (2017) 1351–1360.
[16] A.I. Ivanets, V. Srivastava, M.Yu. Roshchina, M. Sillanpaa, V.G. Prozorovich, V.V. Pankov, Magnesium ferrite nanoparticles as a magnetic sorbent for the removal of Mn^{2+}, Co^{2+}, Ni^{2+} and Cu^{2+} from aqueous solution, Ceram. Int., 44 (2018) 9097–9104.
[17] S.M. Yakout, M.R. Hassan, M.I. Aly, Synthesis of magnetic alginate beads based on magnesium ferrite ($MgFe_2O_4$) nanoparticles for removal of Sr (II) from aqueous solution: kinetic, equilibrium and thermodynamic studies, Wat. Sci. Tech., 77 (2018) 2714–2722.
[18] V.M. Fedorova, S.A. Kobets, L.N. Puzyrnaya, G.N. Pshinko, A.A. Kosorukov, Clinoptilolite/Fe_3O_4: a magnetic sorbent for removing ^{90}Sr from Aqueous Media, Radiochemistry., 59 (2017) 495–499.
[19] K. Ma, Q. Wang, Q. Rong, D. Zhang, S. Cui, Jing Yang, Preparation of magnetic carbon/Fe_3O_4 supported zero-valent iron composites and their application in Pb(II) removal from aqueous solutions, Wat. Sci. Technol., 76 (2017) 2680–2689.
[20] M.S. Samuel, Sk. S. Shah, V. Subramaniyan, T. Qureshi, J. Bhattacharya, N.D.P. Singh, Preparation of graphene oxide/chitosan/ferrite nanocomposite for chromium(VI) removal from aqueous solution, Int. J. Biol. Macromol., 119 (2018) 540–547.
[21] K. Deepa, C. Prasad, N.V.V. Jyothi, M. Naushad, S. Rajendran, S. Karlapudi, S. Himagirish Kumar, Adsorptive removal of Pb(II) metal from aqueous medium using biogenically synthesized and magnetically recoverable core-shell structured AM@Cu/Fe_3O_4 nano composite, Desal. Wat. Treat., 111 (2018) 278–285.
[22] K.L. Bhowmik, A. Debnath, R. Kumar Nath, B. Saha, Synthesis of $MnFe_2O_4$ and Mn_3O_4 magnetic nanocomposites with enhanced properties for adsorption of Cr(VI): artificial neural network modeling, Wat. Sci. Technol., 76 (2017) 3368–3378.
[23] S. Guo, J. Zhang, X. Li, F. Zhang, X. Zhu, Fe_3O_4-CS-L: a magnetic core-shell nano adsorbent for highly efficient methyl orange adsorption, Wat. Sci. Tech., 77 (2018) 628–637.
[24] T. Luo, L. Qu, X. Hou, X. Liu, S. Wang, Y. Wu, Preparation of 3-dimensional flower-like $NiFe_2O_4$ with enhanced adsorptive performance for water contaminants, J. Alloys. Compd., 727 (2017) 484–490.
[25] B.R. Vergis, R.H. Krishna, N. Kottam, B.M. Nagabhushana, R. Sharath, B. Darukaprasad, Removal of malachite green from aqueous solution by magnetic $CuFe_2O_4$ nanoadsorbent synthesized by one pot solution combustion method, J Nanostructure Chem., 8 (2018) 1–12.
[26] K. Cai, W. Shen, B. Ren, J. He, S. Wu, W. Wang, A phytic acid modified $CoFe_2O_4$ magnetic adsorbent with controllable morphology, excellent selective adsorption for dyes and ultra-strong adsorption ability for metal ions, Chem. Eng. J., 330 (2017) 936–946.
[27] A. Sengupta, R. Rao, D. Bahadur, Zn^{2+}–silica modified cobalt ferrite magnetic nanostructured composite for efficient adsorption of cationic pollutants from water, ACS. Sust. Chem. Eng., 5 (2017) 1280–1286.
[28] T. Tatarchuk, M. Bououdina, N. Paliychuk, I. Yaremiy, V. Moklyak, Structural characterization and antistructure modeling of cobalt-substituted zinc ferrites, J. Alloys. Compd., 694 (2017) 777–791.

[29] D.L. Postai, C.A. Demarchi, F. Zanatta, D.C.C. Melo, C.A. Rodrigues, Adsorption of rhodamine B and methylene blue dyes using waste of seeds of *Aleurites Moluccana*, a low cost adsorbent, Alex. Eng. J., 55 (2016) 1713–1723.
[30] M. Ghasemi, M. Naushad, N. Ghasemi, Y. Khosravi-fard, Adsorption of Pb(II) from aqueous solution using new adsorbents prepared from agricultural waste: adsorption isotherm and kinetic studies, J. Ind. Eng. Chem, 20 (2014) 2193–2199.
[31] K. Rama Krishna, K. Vijaya Kumar, D. Ravinder, Structural and electrical conductivity studies in nickel-zinc ferrite, Adv. Mater. Phys. Chem., 2 (2012) 185–191.
[32] S.G.C. Fonseca, L.S. Neiva, M.A.R. Bonifácio, P.R. Cunha, U.C. Silva, J.B.L. Oliveira, Tunable magnetic and electrical properties of cobalt and zinc ferrites $Co_{1-x}Zn_xFe_2O_4$ synthesized by combustion route, Mater. Res., 21 (3) (2018) e20170861.
[33] B.R. Babu, K.V. Ramesh, M.S.R. Prasad, Y. Purushotham, Structural, magnetic, and dielectric properties of $Ni_{0.5}Zn_{0.5}Al_xFe_{2-x}O_4$ nanoferrites, J. Supercond. Nov. Magn., 29 (2016) 939–950.
[34] J.R. Macdonald, Impedance Spectroscopy: Emphasizing Solid Materials and Systems, New York: Wiley-Interscience, 1987
[35] G. Umapathy, G. Senguttuvan, L.J. Berchmans, V. Sivakumar, Structural, dielectric and AC conductivity studies of Zn substituted nickel ferrites prepared bycombustion technique, J. Mater. Sci: Mater. Electron., 27 (2016) 7062–7072.
[36] M. Stoia, C. Muntean, B. Militaru, $MnFe_2O_4$ nanoparticles as new catalyst for oxidative degradation of phenol by peroxydisulfate, J. Environ. Sci., 53 (2017) 269–277.
[37] K.Y. Foo, B.H. Hameed, Insights into the modeling of adsorption isotherm systems, Chem. Eng. J., 156 (2010) 2–10.
[38] I. Langmuir, The adsorption of gases on plane surfaces of glass, mica and platinum., J. Am. Chem. Soc., 40 (1918) 1361–1403.
[39] M. Naushad, Surfactant assisted nano-composite cation exchanger: development, characterization and applications for the removal of toxic Pb^{2+} from aqueous medium, Chem. Eng. J., 235 (2014) 100–108.
[40] H.M.F. Freundlich, Adsorption in solution, Z. Phys. Chem., 57 (1906) 385–470.
[41] M. Ghasemi, M. Naushad, N. Ghasemi, Y. Khosravi-fard, A novel agricultural waste based adsorbent for the removal of Pb(II) from aqueous solution: kinetics, equilibrium and thermodynamic studies, J. Ind. Eng. Chem, 20 (2014) 454–461.
[42] J. Portier, G. Campet, J. Etourneau, M.C.R. Shastry, B. Tanguy, A simple approach to materials design: role played by an ionic-covalent parameter based on polarizing power and electronegativity, J. Alloys. Compd., 209 (1994) 59–64.
[43] M. Lenglet, Iono-covalent character of the metal-oxygen bonds in oxides: a comparison of experimental and theoretical data, Act. Passive. Electron. Compon., 27 (2004) 1–60.
[44] R.D. Shannon, Revised effective ionic radii and systematic studies of interatomic distances in halides and chalcogenides, Acta Cryst., A32 (1976) 751–767.
[45] Y. Zhang, Electronegativities of elements in valence states and their applications. 1. Electronegativities of elements in valence states, Inorg. Chem., 21 (1982) 3886–3889.